Copyright © 2011 by the Genetics Society of America
DOI: 10.1534/genetics.110.125575

Sustained and Rapid Chromosome Movements Are Critical for Chromosome Pairing and Meiotic Progression in Budding Yeast

Megan Sonntag Brown, Sarah Zanders[1] and Eric Alani[2]

Department of Molecular Biology and Genetics, Cornell University, Ithaca, New York 14853

Manuscript received December 1, 2010
Accepted for publication February 5, 2011

ABSTRACT

Telomere-led chromosome movements are a conserved feature of meiosis I (MI) prophase. Several roles have been proposed for such chromosome motion, including promoting homolog pairing and removing inappropriate chromosomal interactions. Here, we provide evidence in budding yeast that rapid chromosome movements affect homolog pairing and recombination. We found that *csm4*Δ strains, which are defective for telomere-led chromosome movements, show defects in homolog pairing as measured in a "one-dot/two-dot tetR-GFP" assay; however, pairing in *csm4*Δ eventually reaches near wild-type (WT) levels. Charged-to-alanine scanning mutagenesis of *CSM4* yielded one allele, *csm4-3*, that confers a *csm4*Δ-like delay in meiotic prophase but promotes high spore viability. The meiotic delay in *csm4-3* strains is essential for spore viability because a null mutation (*rad17*Δ) in the Rad17 checkpoint protein suppresses the delay but confers a severe spore viability defect. *csm4-3* mutants show a general defect in chromosome motion but an intermediate defect in chromosome pairing. Chromosome velocity analysis in live cells showed that while average chromosome velocity was strongly reduced in *csm4-3*, chromosomes in this mutant displayed occasional rapid movements. Lastly, we observed that *spo11* mutants displaying lower levels of meiosis-induced double-strand breaks showed higher spore viability in the presence of the *csm4-3* mutation compared to *csm4*Δ. On the basis of these observations, we propose that during meiotic prophase the presence of occasional fast moving chromosomes over an extended period of time is sufficient to promote WT levels of recombination and high spore viability; however, sustained and rapid chromosome movements are required to prevent a checkpoint response and promote efficient meiotic progression.

CELLS that enter meiosis undergo a single round of DNA replication followed by two divisions to yield haploid gametes, such as sperm and eggs in humans and spores in baker's yeast. Accurate segregation of chromosomes at the meiosis I (MI) and II (MII) divisions is a critical part of this process. Improper segregation can lead to aneuploidy, which in humans is a leading cause of infertility, miscarriages, and mental retardation (Hassold and Hunt 2001). One of the main causes of aneuploidy is nondisjunction of homologous chromosomes during MI. In most organisms, at least one crossover per homolog pair is essential for MI disjunction (Roeder 1997; Zickler and Kleckner 1999). Chromosome nondisjunction can occur if there are too few or too many crossovers or if crossovers are not properly placed, such as in close proximity to centromeres and telomeres (Hassold and Hunt 2001; Rockmill *et al.* 2006; Lacefield and Murray 2007). In the latter case, crossing over far from the centromere increases the likelihood of chromosomes segregating to the same spindle pole, resulting in aneuploidy (Lacefield and Murray 2007; Martinez-Perez and Colaiácovo 2009).

In baker's yeast, crossing over is initiated in meiosis by the formation of Spo11-dependent DNA double strand breaks (DSBs) (Keeney 2001). These breaks can be repaired as either crossovers or noncrossovers, with ~60% of the 140–170 DSBs processed as crossovers (Buhler *et al.* 2007; Mancera *et al.* 2008). In the interference-dependent crossover pathway, which leads to more widely spaced crossovers, DSBs are processed to form single-end invasion intermediates (SEIs) that result from the invasion of a DSB end into an intact homolog. These intermediates undergo second-end capture with the intact homolog to form double Holliday junctions (dHJs) that are ultimately resolved to form crossovers (Schwacha and Kleckner 1995; Allers and Lichten 2001; Börner *et al.* 2004; Lao *et al.* 2008).

During meiotic prophase in *Saccharomyces cerevisiae*, distinct chromosome motions are observed, which have been hypothesized to promote chromosome disjunction at MI. At the end of leptotene, telomeres attach to the nuclear envelope and move toward the spindle pole body, forming a bouquet-like structure (Trelles-

Supporting information is available online at http://www.genetics.org/cgi/content/full/genetics.110.125575/DC1.

[1]*Present address:* Division of Basic Sciences, Fred Hutchinson Cancer Research Center, Mail Stop A2-025, P.O. Box 19024, Seattle, WA 98109-1024.

[2]*Corresponding author:* Department of Molecular Biology and Genetics, Cornell University, 459 Biotechnology Bldg., Ithaca, NY 14853-2703. E-mail: eea3@cornell.edu

Sticken *et al.* 1999, 2005). This bouquet structure is transient, but has been proposed to play a role in meiotic crossing over, since mutants in a variety of organisms that are defective for bouquet formation show defective or altered steps in recombination (Chua and Roeder 1997; Yamamoto *et al.* 1999; Niwa *et al.* 2000; Golubovskaya *et al.* 2002; Bass 2003; Harper *et al.* 2004; Davis and Smith 2006; Wu and Burgess 2006; Kosaka *et al.* 2008; Wanat *et al.* 2008). The synaptonemal complex (SC), a proteinaceous structure that holds homologous chromosomes together and acts as a scaffold for crossing over, begins to form at the same time as bouquet formation (Page and Hawley 2004; Joseph and Lustig 2007). After the bouquet stage ends, in early zygotene in baker's yeast, rapid prophase movements led by dispersed telomeres ensue concurrently with extension of the SC and continue into pachytene (Scherthan *et al.* 2007; Conrad *et al.* 2008; Koszul *et al.* 2008). The SC dissolves in diplotene, leaving chiasmata, the physical manifestations of crossovers, intact (Harper *et al.* 2004). The chromosomes then proceed through anaphase and complete the MI division.

Many roles have been proposed for telomere-led movements seen in zygotene and pachytene. Studies have found that mutants defective in these movements have a small increase in ectopic recombination, suggesting motion may prevent ectopic interactions (Chua and Roeder 1997; Goldman and Lichten 2000). Telomere-led movements have been proposed to untangle nonhomologous chromosomes, possibly from interlocks formed during SC formation (Rasmussen 1986; Scherthan *et al.* 1994; Wanat *et al.* 2008; Storlazzi *et al.* 2010). These movements have also been proposed to promote homolog pairing, SC formation, and sister chromatid cohesion (Scherthan *et al.* 1996; Rockmill and Roeder 1998; Harper *et al.* 2004; Sato *et al.* 2009).

In budding yeast, Mps3, Ndj1, and Csm4 are required for bouquet formation and zygotene to pachytene telomere-led movements (Trelles-Stricken *et al.* 2000; Conrad *et al.* 2007; Wanat *et al.* 2008). Mps3 interacts with Ndj1, which is a meiosis-specific protein that localizes to telomeres (Chua and Roeder 1997; Conrad *et al.* 1997). Both Ndj1 and Mps3, a SUN domain nuclear envelope protein, are required to attach telomeres to the nuclear envelope, one of the key steps in forming a bouquet (Conrad *et al.* 2007). Csm4, a cytoplasmic tail-anchored protein, interacts with both Ndj1 and Mps3 (Rabitsch *et al.* 2001; Conrad *et al.* 2008; Kosaka *et al.* 2008). Csm4 is not needed for telomere attachment to the nuclear envelope, but is required for rapid telomere-led movements during meiosis (Conrad *et al.* 2008; Kosaka *et al.* 2008; Koszul *et al.* 2008; Wanat *et al.* 2008). The cytoskeleton is also necessary for chromosome motion, because disruption of microtubules in *Schizosaccharomyces pombe*, or actin in budding yeast, arrests chromosome motion and prevents bouquet formation (Yamamota *et al.* 1999; Trelles-Sticken *et al.* 2005; Chikashige *et al.* 2007; Scherthan *et al.* 2007; Koszul *et al.* 2008). The attachment of chromosomes through Mps3, Ndj1, and Csm4 to the actin cytoskeleton in budding yeast appears to be passive. Telomeres are thought to associate with dynamic cytoplasmic actin cables that hug the nucleus, with lead chromosome(s) directing the movement of other chromosomes (Conrad *et al.* 2008; Koszul *et al.* 2008). In support of this notion, chromosome motion occurs at a similar speed to actin cable extension (~0.3 μm/sec; Yang and Pon 2002).

Previous studies have shown Csm4 is important for MI disjunction of chromosomes (Kosaka *et al.* 2008; Wanat *et al.* 2008). The *csm4*Δ mutation confers a spore viability defect (60–65% compared to ~90–95% for wild type, WT) with patterns of spore viability (prevalence of 4, 2, and 0 viable spores) and chromosome segregations in two-spore viable tetrads consistent with MI nondisjunction. Crossing over, however, is not decreased, but occurs at higher than WT levels (Wanat *et al.* 2008). Furthermore, analysis of two spore viable tetrads that had undergone MI nondisjunction showed similar crossover levels to WT but differences in crossover placement (Wanat *et al.* 2008). Lastly, all aspects of recombination after the initiation of DSBs are delayed in *csm4*Δ, resulting in an overall 4- to 5-hr delay in completion of MI.

In this study, we identified a defect in homolog pairing in *csm4*Δ. We then analyzed a set of charged-to-alanine scanning mutagenesis alleles to tease apart the role of chromosome motion in pairing. We found one allele, *csm4-3*, that conferred high spore viability, but an MI delay similar to the null. We further characterized this allele, showing it confers a defect in chromosome motion and pairing, but each to a lesser degree than the null. Our data are consistent with sustained and rapid chromosome movements being required in meiosis to promote chromosome pairing and efficient meiotic progression.

MATERIALS AND METHODS

Media and yeast strains: Yeast strains were grown at 30° on YPD (YP, yeast and peptone plus D, dextrose) supplemented with complete amino acid mix (Rose *et al.* 1990). Sporulation plates and other media have been described previously (Wach *et al.* 1994; Wanat *et al.* 2008). When appropriate, minimal selective media, synthetic complete media supplemented with 5 μM copper sulfate, and YPD supplemented with complete amino acid mix and 3 mg/liter cycloheximide were used (Rose *et al.* 1990). When required, geneticin (Invitrogen) and hygromycin B (Calbiochem) were included in YPD media as previously described (Goldstein and McCusker 1999).

Parental strains (supporting information, Table S1) in this work included the isogenic SK1 strain NHY943/NHY942 (de los Santos *et al.* 2003), the congenic SK1 strain EAY1108/EAY1112 (Tsubouchi and Roeder 2003; Argueso *et al.* 2004), Nup49-GFP, and Zip1-GFP SK1 strains (Koszul *et al.* 2008), one-dot/two-dot tetR-GFP pairing assay SK1 strains (Tóth *et al.* 2000; Alexandru *et al.* 2001; Marston *et al.*

2004; Brar *et al.* 2009), and SK1 *spo11* hypomorph strains (Diaz *et al.* 2002; Henderson and Keeney 2004; Martini *et al.* 2006). The *spo11(Y135F)-HA3His6/spo11-HA* genotype described by Keeney and colleagues (Martini *et al.* 2006) is referred to in this study as *spo11-HA/yf*.

Yeast strains were constructed using standard transformation protocols (Gietz *et al.* 1995) and integration events were confirmed using PCR primers flanking insertion regions. Site-specific mutations in *csm4* were also confirmed by DNA sequencing of *CSM4* DNA PCR amplified from the strain of interest. The *csm4*Δ allele contains a complete deletion of the open reading frame. *csm4-3* contains two mutations, K22A and K24A. Other allele information can be found in Table S1.

Alanine scanning mutagenesis: The *CSM4* one-step integrating vector pEAA381 (*CSM4::KANMX, URA3, ARSH4 CEN6*) was modified by Quick Change (Stratagene, La Jolla, CA) site-directed mutagenesis to create 19 *csm4* derivatives. The entire *CSM4* open reading frame, including 400 bp upstream, was sequenced in the mutant plasmids to ensure that only the desired amino acid changes were introduced. pEAA381 and mutant derivatives were digested with *Sac*I and *Sph*I to release a DNA fragment containing *CSM4* (or *csm4* alleles), the *KANMX* marker, and DNA sequence downstream of *CSM4*. The *KANMX* marker is located between the CSM4 open reading frame and the downstream *CSM4* sequence. The DNA fragments were then transformed into yeast and integration of *CSM4::KANMX* and *csm4::KANMX* derivatives was confirmed by PCR analysis and DNA sequencing. The DNA sequences of the oligonucleotides used to create the *csm4* alleles and the resulting plasmids are available upon request.

Meiotic time courses: Meiotic time courses were performed as follows: 0.35 ml of a saturated YPD overnight culture of the desired strain was inoculated into 200 ml YPA (YP + 2% potassium acetate) plus complete amino acid mix and grown for 16–17 hr at 30°. Cells in the YPA culture were spun down, washed once in 100 ml 1.0% potassium acetate, resuspended in 100 ml 1.0% potassium acetate, and then incubated with vigorous shaking at 30°. All strains for a single time course were grown in the same batch of media under identical conditions. The *csm4* alleles were initially analyzed in the Nup49-GFP background. Strains bearing *spo11* and *rad17*Δ mutations were analyzed in the NH942/NH943 and EAY1108/EAY1112 strain backgrounds, respectively.

Aliquots of cells at specific time points were DAPI stained to determine the percentage of cell that completed at least the first meiotic division (cells in which 2, 3, or 4 nuclei were observed by DAPI staining; MI ± MII; Galbraith *et al.* 1997). Cells were visualized using Olympus BX60 microscope and at least 150 cells were counted for each time point. For each strain the time required for 40% cells to have completed MI was recorded and mutant phenotypes were presented with respect to the delay (hr) in completing MI relative to WT.

Tetrad dissection and analysis: Diploids were constructed using the zero growth mating protocol (Argueso *et al.* 2003). Haploid parental strains were mated for 4–5 hr on YPD plates before being spread onto sporulation plates. The plates were incubated at 30° for at least 2 days before dissection. All strains were dissected onto synthetic complete media. Colonies derived from germinated spores were incubated at 30° for 2–3 days before being replica plated to appropriate selective media. Replica plates were scored after a 1-day incubation at 30°. The distributions of each tetrad type and map distances were calculated using RANA software (Argueso *et al.* 2004).

Live cell imaging: Cells were observed at room temperature using a Zeiss Imager M2 fluorescent microscope equipped with DAPI, GFP, and TexRed filters, an Axiocam MR camera, and a ZipL Piezo Z device for acquiring *z*-stacks. Images were acquired using Axiovision software.

Nup49-GFP motion assays were conducted in live WT, *csm4*Δ, and *csm4-3* cells (Koszul *et al.* 2008). Time courses were performed as described above. In initial studies, samples obtained from each time point were incubated at 4° overnight prior to analyzing Nup49-GFP motion by light microscopy. These assays have since been repeated in the absence of the 4° incubation step; no significant differences were seen in Nup49-GFP motion using the two methods. To maximize aeration of cells, at each time point 3-μl aliquots of vortexed cells were placed on an untreated glass slide and then covered with a cover slip. Only cells located near air bubbles were analyzed (Koszul *et al.* 2009). Images were taken at 1-sec intervals with exposure times for Nup49-GFP cells ranging from 600 to 700 msec. Zip1-GFP time courses (Koszul *et al.* 2008) were analyzed in the same manner as in the Nup49-GFP experiments, but without including the 4° incubation step. The exposure time for Zip1-GFP cells was 600 msec. Chromosome velocities in the Zip1-GFP time courses were calculated using a manual tracking plugin on ImageJ. Clearly isolated chromosomes in a cell were manually marked at the telomere and monitored at each exposure time for at least 15 consecutive frames. This resulted in at least 15 velocity measurements for each chromosome. Average speeds for each chromosome were calculated from the mean of the 15–25 velocity measurements. The maximum velocity seen between frames (~1-sec intervals) for each chromosome was determined to be the maximum for that chromosome. Thirty chromosomes from 30 independent cells were analyzed for each genotype.

One-dot/two-dot tetR-GFP time courses were performed, similar to Brar *et al.* (2009) as follows: 0.35 ml of a saturated overnight YPD culture of the desired strain was inoculated into 100 ml YPA and grown for 16–17 hr at 30°. The YPA culture was subsequently washed once in 1% KAc, resuspended in 50 ml 1% KAc, and then incubated with vigorous shaking at 30°. Cell aliquots were taken at specific time points and examined with the GFP filter in *z*-stacks (~20 planes separated by 0.3 μm) with an exposure time of 150 msec. See *Media and yeast strains* and Table S1 for strain details.

RESULTS

Csm4 acts in chromosome pairing: We used a one-dot/two-dot tetR-GFP assay developed by the Amon laboratory (Brar *et al.* 2009) to test whether *csm4*Δ mutants display a defect in homolog pairing in meiosis. Diploid strains analyzed in this assay contain an array of tet operator (*tetO*) sequences in both copies of a particular locus (*LYS2, TELV*, and *CENV*). These strains also contain a tet repressor (tetR)-GFP fusion construct present at another location. A visible GFP focus is seen when tetR binds the *tetO* array. Pairing is assayed in unfixed cells by determining whether one (paired) or two (unpaired) clear GFP dots are observed (Figure S1). Strains used in the pairing assays contain the *ndt80*Δ mutation (*NDT80* is required for exit from pachytene) so that maximum pairing levels can be assessed (Weiner and Kleckner 1994; Peoples *et al.* 2002). It is important to note that in our study, only strains used for live cell imaging contain the *ndt80* mutation. Cells enter meiosis ($T = 0$) with a high level of one-dot cells, which is thought to be due to residual somatic pairing and/or the Rabl orientation, where centromeres cluster during interphase (Loidl *et al.* 1994; Weiner and Kleckner,

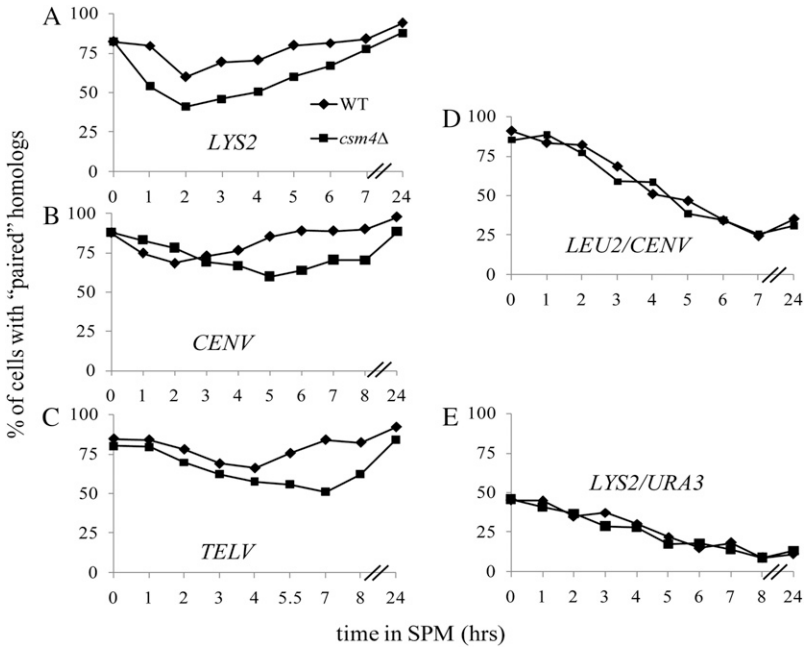

FIGURE 1.—Chromosome pairing is defective in *csm4*Δ. Chromosome pairing was assessed in diploid SK1 strains ectopically expressing tetR-GFP and bearing *tet0* arrays at homologous positions (BRAR *et al.* 2009; MATERIALS AND METHODS). Homologs were considered paired when only one GFP dot was observed and were considered unpaired when two clear GFP dots were seen (Figure S1). Cells were analyzed using *z*-stacks to visualize the entire cell volume. (A, B, and C) Representative time courses (chosen from four to eight independent experiments) with *tetO* arrays at *LYS2* (A), *CENV* (B), and *TELV* (C). Pairing was considered maximum in these *ndt80*Δ strains at $T = 24$ hr. (D and E) Representative time courses demonstrating nonhomologous pairing, with one *tetO* array at *LEU2* and another at *CENV* (D) and one at *LYS2* and another at *URA3* (E).

1994; BURGESS *et al.* 1999). The one-dot phenotype is lost in the first few hours of meiosis, before *SPO11*-dependent pairing is observed (see BRAR *et al.* 2009 and Figure 1 for examples). Here, we use the term "pairing" loosely to incorporate a wide range of homolog interactions, ranging from the initial alignment of homologs (400 nM; ZICKLER and KLECKNER 1999) to DNA interactions (*e.g.*, SEI formation) that occur after initial homolog interactions have occurred. Pairing was assayed at three distinct sites in the genome: *LYS2*, located on an arm of chromosome II, and *TELV* and *CENV*, located near a telomere and the centromere of chromosome V, respectively. Pairing was also assessed in strains containing *tetO* arrays at nonhomologous sites (*LEU2* and *CENV*; *URA3* and *LYS2*). These strains allow us to visualize the loss of one-dot cells through meiotic prophase. They also serve as controls to measure the frequency of GFP dots that colocalize by chance.

We analyzed homolog pairing in WT and *csm4*Δ cells at *LYS2*, *CENV*, and *TELV* and observed a pairing defect in *csm4*Δ (Figure 1). Pairing occurred with dynamics similar to WT for the first few hours after entry into sporulation media; however, *csm4*Δ strains consistently reached a lower pairing level at all three loci (Figure 1, A, B, and C; Figure S2). Furthermore, while *csm4*Δ reached near WT levels of pairing by 24 hr, there was a delay in reaching maximal pairing levels at all three loci. This delay could be due solely to the 4- to 5-hr meiotic delay in *csm4*Δ; however, this appears unlikely, because as discussed below, an allele with the same meiotic delay progressed through pairing more rapidly than the null. The slightly lower values of homolog pairing at 24 hr may be due to the slight sporulation defect seen in *csm4*Δ (WANAT *et al.* 2008); one possibility is that a small percentage of *csm4*Δ cells do not proceed to the homolog pairing stage of meiosis. However, *csm4*Δ showed a phenotype identical to WT when looking at nonhomologous loci (Figure 1, D and E). It is important to note that the initial high levels of pairing observed in the *LEU2/CENV* strains is likely due to *LEU2* being near a centromere and thus showing residual vegetative pairing with *CENV* due to the Rabl orientation. Our data suggest that *csm4*Δ does not have a defect in removing the pairing seen between nonhomologous chromosomes at early stages in meiosis. The data also suggest that the *csm4*Δ strains do not have an increased likelihood in random overlap of GFP dots.

Analysis of *csm4* alleles: To further investigate whether the rapid chromosome motion that takes place during meiotic prophase is necessary for homolog pairing and spore viability, and to determine whether these phenotypes can be separated, we created a set of 19 alleles of *CSM4* by charged-to-alanine scanning mutagenesis (Figure 2A). This approach allowed mutagenesis of a large number of residues in Csm4 with the expectation that protein–protein interactions would involve solvent-exposed residues. *csm4*Δ has a low spore viability (~60%) and a long meiotic delay of 4–5 hr compared with WT. We analyzed meiotic delay and spore viability for these 19 mutants and found a wide range of spore viabilities, ranging from the null (60%) to WT (90%), as well as a wide range of meiotic delays, from no delay to a null-like 5-hr delay (Table 1; MATERIALS AND METHODS). We found that the null alleles grouped into two regions of the proteins, from amino acids 31–66 and 100–111. This suggests that these two regions are important for function and may contain an interaction domain for Ndj1 or Mps3, or a yet-to-be discovered interacting protein. As

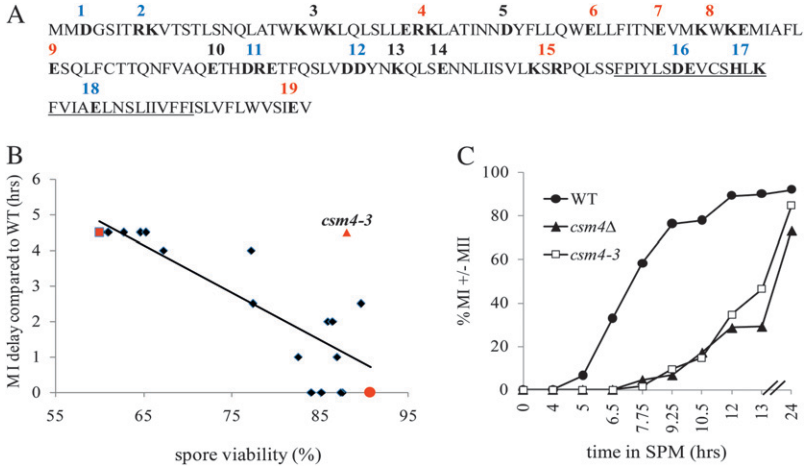

FIGURE 2.—*csm4-3* is a separation of function allele. (A) Amino acids in the Csm4 polypeptide were mutated to alanine residues as indicated in boldface type. The allele designation is shown above each set of amino acid substitutions. The putative transmembrane domain is underlined near the C terminus. Alleles that conferred a WT phenotype as measured by spore viability and timing of the MI division (MATERIALS AND METHODS) are shown in blue; alleles that displayed a null phenotype in these assays are shown in red. Intermediate alleles are shown in black. (B) The phenotypes of *csm4* alleles (Table 1) are presented in a graph in which spore viability is plotted *vs.* MI delay, relative to WT, in completing the MI division. Cells with two, three, or four nuclei were counted as having completed M1 (MI ± MII). The phenotypes of WT (red circle) and *csm4*Δ (red square) are indicated. *csm4-3*, a separation-of-function allele, is highlighted (red triangle). (C) Representative time course showing the completion of the MI division (MI ± MII) in WT, *csm4*Δ, and *csm4-3* strains.

expected, a negative correlation was seen between meiotic delay and spore viability; as spore viability increased, the meiotic delay decreased (Figure 2B). One strain, *csm4-3*, is an outlier to this pattern, showing high spore viability and sporulation, but a meiotic delay similar to the null (Figure 2C).

Chromosome motion is strongly reduced in *csm4-3*: Telomere-led chromosome motion was studied for a subset of the *csm4* mutants. Strains that showed near WT spore viability and no meiotic delay (*csm4-1, -2, -12, -17*, and *-18*) or those that showed null-like spore viability and a long meiotic delay (*csm4-4, -6, -9*, and *-15*) were not analyzed further (Table 1). Initially we analyzed motion in strains containing Nup49-GFP, a nuclear pore protein that marks the nuclear envelope (BELGAREH and DOYE 1997). When chromosome movement occurs in meiotic prophase, chromosomes are rocketed into the nuclear envelope; this movement is clearly seen in WT strains expressing Nup49-GFP (Figure 3A; KOSZUL *et al.* 2008). The nuclear envelope distortions were seen beginning in zygotene and reached maximum levels during pachytene (4–6 hr after induction of meiosis; KOSZUL *et al.* 2008). Cells were assigned as having chromosome motion on the basis of the presence or absence of nuclear envelope distortions (Table 1). Mutants with null levels of Nup49-GFP motion (nuclear envelope appears spherical in *csm4-3, -7, -8*, and *-14*) all have long meiotic delays (ranging from 2.5 to 4.5 hr), but their spore viabilities varied greatly, from 63 to 88%. Mutants with intermediate to WT levels of motion (occasional nuclear envelope distortions in *csm4-5, -10, -11, -13, -16*, and *-19*) displayed intermediate to WT levels of spore viability (81–89%); however, meiotic delays in these mutants ranged from no delay to a 4-hr delay.

As mentioned above, *csm4-3* strains retain high spore viability but display a null-like MI delay and *csm4*Δ-like defect in the Nup49-GFP chromosome motion assay (Figure 3A). Since nuclear envelope distortions provide only an indirect measure of chromosome motion, we directly examined chromosome motion in strains expressing Zip1-GFP. Zip1 loads onto chromosomes in foci early in meiosis and then localizes along the central element in fully synapsed chromosomes during zygotene and pachytene (CHUA and ROEDER 1998; BÖRNER *et al.* 2008). Such a localization pattern is ideal for measuring chromosome motion (SCHERTHAN *et al.* 2007; CONRAD *et al.* 2008; KOSAKA *et al.* 2008; KOSZUL *et al.* 2008; WANAT *et al.* 2008). In WT strains in zygotene and pachytene expressing Zip1-GFP (T = 4–6 hr after meiotic induction), chromosomes rapidly move within the nucleus, at rates up to 1.2 μm/sec, with an average velocity of 0.30 ± 0.08 (standard deviation, SD) μm/sec (Figure 3B). Similar to previous studies (CONRAD *et al.* 2008; KOSZUL *et al.* 2008), chromosome motion is severely reduced in *csm4*Δ with a maximum velocity of 0.39 μm/sec and an average velocity of 0.12 ± 0.03 μm/sec. Chromosomes in *csm4-3* reached a maximum velocity of 0.70 μm/sec and displayed an average velocity of 0.18 ± 0.04 μm/sec (Figure 3B), which differed significantly from the null ($P < 0.0001$ by one-sided Mann–Whitney test), mostly due to the contribution of a few chromosomes moving rapidly in *csm4-3* (Figures 3, 4, and 5). The presence of occasional, fast moving chromosomes in *csm4-3* is clearly seen in an analysis of chromosome velocity in consecutive 1-sec intervals for three representative chromosomes of each genotype (Figure 5). For WT, 26% of chromosome movements were >0.4 μm/sec; in contrast only 9.2 and 0% were above this value in *csm4-3* and *csm4*Δ, respectively. Together these data suggest that high levels of chromosome motion are not essential to achieve WT levels of spore viability.

Homolog pairing is defective in *csm4-3*: *csm4-3* strains show defects in chromosome motion in the Nup49-GFP and Zip1-GFP assays. If WT levels of chromosome movements are important for homolog pairing in meiosis, we would expect *csm4-3* strains to show pairing defects. We

TABLE 1

Characterization of *csm4* mutants with respect to spore viability, completion of the meiosis I division, nuclear envelope distortions, and genetic map distances

Strain	% SV (*n*)	MI delay (hr)	NE distortions	Map distance in cM (*n*)
WT	91 (120)	0	+	101 (1068)[a]
*csm4*Δ	60 (120)	4.5	−	146 (531)[a]
*CSM4/csm4*Δ	90 (240)	ND	+	109 (160)
csm4-1	88 (100)	0	ND	ND
csm4-2	85 (220)	0	ND	ND
csm4-3	88 (360)	4.5	–	126 (238)
csm4-4	61 (100)	4.5	ND	ND
csm4-5	86 (260)	2.0	±	141 (100)
csm4-6	65 (60)	4.5	ND	ND
csm4-7	67 (40)	4.0	−	ND
csm4-8	63 (100)	4.5	−	ND
csm4-9	60 (140)	4.5	ND	ND
csm4-10	82 (240)	1.0	±	124 (120)
csm4-11	89 (200)	0	+	ND
csm4-12	87 (60)	0	ND	ND
csm4-13	83 (420)	2.0	±	140 (200)
csm4-14	77 (280)	2.5	−	146 (160)
csm4-15	65 (60)	4.5	ND	ND
csm4-16	89 (320)	2.5	+	147 (200)
csm4-17	87 (160)	1.0	ND	ND
csm4-18	91 (100)	0	ND	ND
csm4-19	78 (380)	4.0	±	141 (160)

Spore viabilities [SV, with the number (*n*) of tetrads dissected], delay in hours in completing MI relative to WT, and the nuclear envelope (NE) distortion phenotype in the Nup49-GFP strain (Table S1) background are shown. +, ±, and – represent WT, intermediate, and defective Nup49-GFP motion, respectively. Cumulative genetic distance between *URA3* and *HIS3* on chromosome XV in EAY1108/EAY1112 derived strains was determined from tetrad data (n = number dissected). Complete tetrad data are provided in Table S2. ND, not determined. See MATERIALS AND METHODS for details.
[a]Data from WANAT *et al.* (2008).

analyzed the *csm4-3* pairing phenotype in the one-dot/two-dot tetR-GFP assay (BRAR *et al.* 2009). As shown in Figure 6, *csm4-3* strains displayed similar kinetics for initial loss of chromosome pairing; however, at later time points, pairing in *csm4-3* occurred more rapidly than in *csm4*Δ, but still slower than seen in WT. Similar to WT and the null, *csm4-3* did not show any difference in dynamics or levels of nonhomologous pairing (Figure 6, D and E). Together these data suggest that *csm4-3* strains are capable of removing nonhomologous interactions as efficiently as WT. In addition, these observations suggest that the pairing defect in *csm4*Δ is not due solely to meiotic progression delays seen in the null, because *csm4-3* displays a delay in completing MI similar to *csm4*Δ, but is more proficient than the null in chromosome pairing.

Chromosome motion is important for meiotic progression: On the basis of the above observations, we hypothesize that WT levels of chromosome motion, while not needed to maintain high spore viability, are important for promoting meiotic progression. To test this, we looked at the phenotype of *csm4*Δ and *csm4-3* mutants in the presence of a deletion of the DNA damage checkpoint protein Rad17. As shown above, both *csm4*Δ and *csm4-3* exhibit 4- to 5-hr delays in completing MI. Previously, WANAT *et al.* (2008) examined physical recombination intermediates that occur in meiosis (DSB, SEI, and dHJ) and found that in *csm4*Δ, recombination steps following DSB formation were delayed. Moreover, each stage was more progressively delayed than the previous step, with the largest delay occurring in the step from DSB to SEI formation. This suggests a major defect occurs in *csm4*Δ strains in an early step in recombination, possibly partner identification or juxtaposition (WANAT *et al.* 2008). The *rad17*Δ mutation was shown previously to eliminate meiotic delays in a variety of mutants, including *dmc1*Δ, *ndj1*Δ, and *pch2*Δ (LYDALL *et al.* 1996; GRUSHCOW *et al.* 1999; WU and BURGESS 2006; WU *et al.* 2010). We found that *rad17*Δ completely rescued the meiotic delay of both *csm4*Δ and *csm4-3* (Figure 7, A and B; WANAT *et al.* 2008); however, spore viability was extremely low in both double mutants (1–3%) compared to 65% in *csm4*Δ and 88% in *csm4-3* (Table 2). These observations suggest that the *csm4-3* mutation elicits a checkpoint response that is required to maintain high spore viability.

One explanation for the poor spore viability phenotype seen in *csm4*Δ is that the mutant is defective in meiotic recombination progression and accumulates a small amount of recombination intermediates that are unrepaired and that elicit the Rad17-dependent (recombination) checkpoint (WANAT *et al.* 2008). The *spo11*Δ mutation rescues the MI delay of many meiotic recombination mutants. In most cases, this phenotype can be explained by *spo11*Δ eliminating the formation of meiosis-induced DSBs and thus preventing the accumulation of DNA recombination intermediates in mutants that activate the Rad17-dependent checkpoint (*e.g.*, LYDALL *et al.* 1996; WU and BURGESS 2006; WU *et al.* 2010). This loss of meiotic DSBs, however, results in spore inviability due to a loss in crossing over. We examined whether lowering the number of DSBs through a *spo11* hypomorph mutation (MARTINI *et al.* 2006) could rescue the meiotic delay phenotypes of *csm4*Δ and *csm4-3*. We used a strain heterozygous for the *spo11-HA* and *spo11-yf-HA* alleles (referred to as *spo11-HA/yf*). This strain makes 30% of WT DSB levels (HENDERSON and KEENEY 2004; MARTINI *et al.* 2006). We analyzed meiotic progression in *csm4*Δ *spo11-HA/yf* and *csm4-3 spo11-HA/yf* by DAPI staining and saw in both cases a partial rescue of the meiotic delay (Figure S3). Interestingly, *spo11-HA/yf* decreased spore viability by roughly the same amount in WT and *csm4-3* strain backgrounds (17% in WT, 18% in *csm4-3*). However, *spo11-HA/yf* reduced spore viability to a greater extent in *csm4*Δ (35%; Table 2). The spore viability in both double mutants showed a pattern indicative of MI

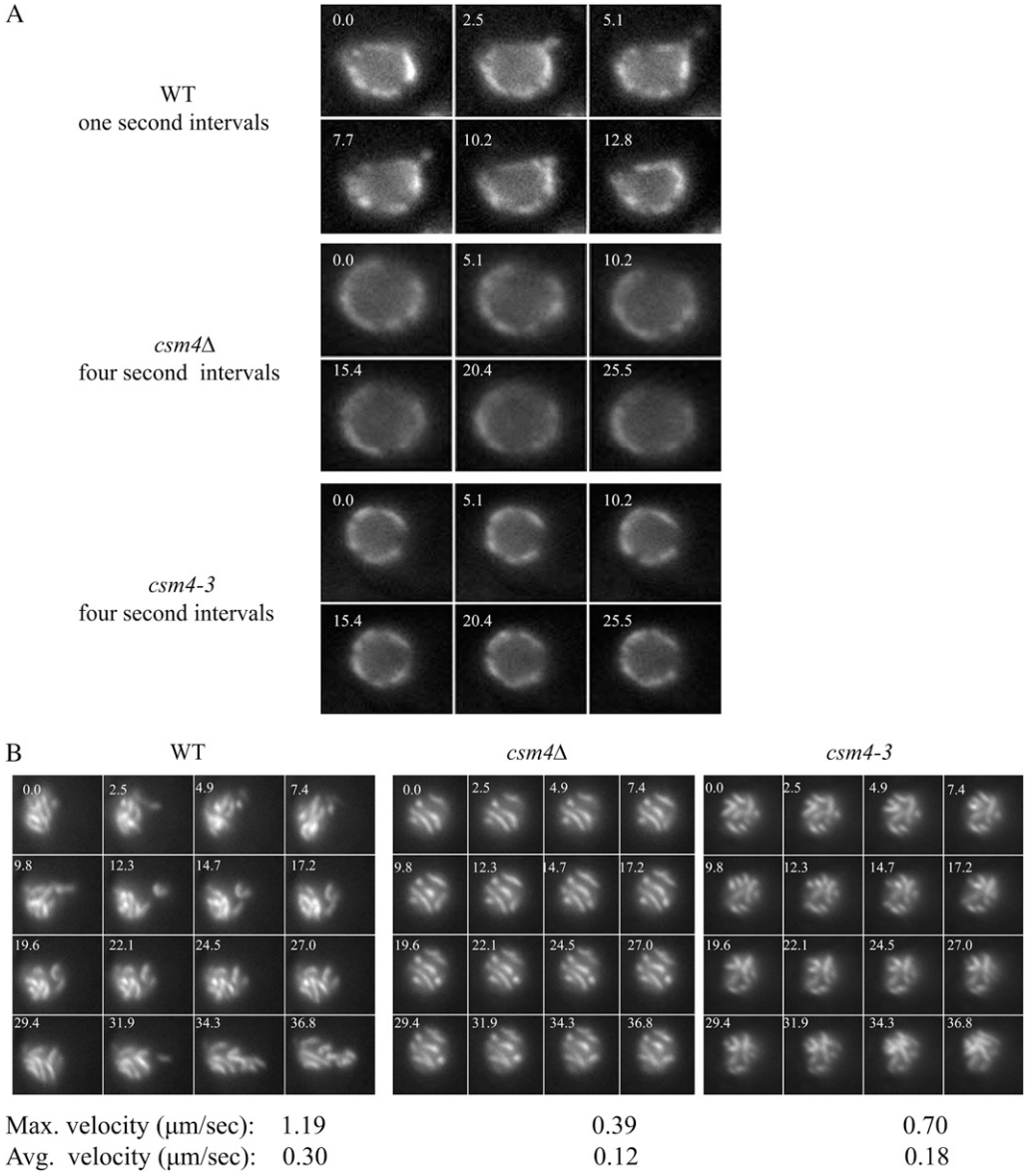

FIGURE 3.—Analysis of *csm4-3* in Nup49-GFP and Zip1-GFP motion assays. (A) Representative time-lapse images of WT, *csm4*Δ, and *csm4-3* cells expressing Nup49-GFP, which marks the nuclear envelope. Images were taken at 1-sec intervals for 30–45 sec. Every other frame is shown for WT; every fourth frame for *csm4*Δ and *csm4-3*. Elapsed time is shown in the upper left corner for each frame. (B) Representative time-lapse images of WT, *csm4*Δ, and *csm4-3* strains expressing Zip1-GFP, which localizes to synapsed chromosomes. Images were taken at 1-sec intervals for 45 sec. Every other frame for a portion of the time lapse is shown (see MATERIALS AND METHODS). Elapsed time is shown in the upper left corner for each frame. Maximum and mean chromosome velocity for all chromosomes analyzed is shown below each genotype in micrometers per second, on the basis of 30 chromosome measurements from 30 different cells across four time courses.

nondisjunction (4, 2, 0 > 3, 1 viable spores; Figure S4). We also measured genetic map distance on three chromosomes (III, VII, and VIII) in *csm4-3 spo11-HA/yf* and *spo11-HA/yf* (Table 2; Table S3). Such an analysis could not be performed in *csm4*Δ *spo11-HA/yf* due to poor spore viability. Map distances in the two mutants were similar across each chromosome (total for all three chromosomes, 159 cM in *csm4-3 spo11-HA/yf vs.* 150 cM in *spo11-HA/yf*).

The partial rescue of the MI delay in *csm4*Δ *spo11-HA/yf* suggests that the *csm4*Δ pairing defect could cause poor or inappropriate repair of recombination intermediates. However, the double mutant analysis does not directly address why spore viability is greatly decreased in *csm4*Δ

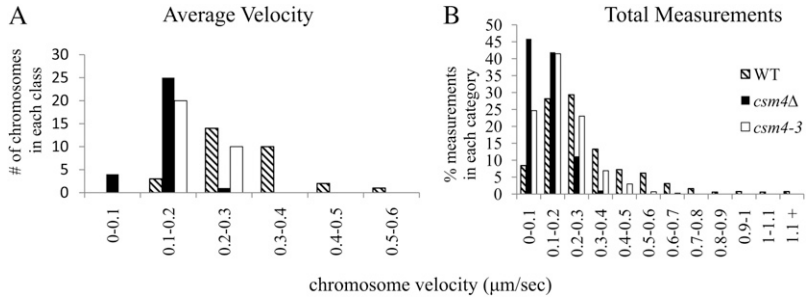

FIGURE 4.—*csm4-3* shows a defect in chromosome motion in cells expressing Zip1-GFP. (A) Distributions of average velocities for each chromosome measured (30 each for WT, *csm4*Δ, and *csm4-3*). Average values for each chromosome were obtained from 15 to 25 velocity measurements determined in 1-sec intervals. (B) Chromosome velocity measurements in 1-sec intervals presented as a percentage of the total number recorded (678, 654, and 738 measurements for WT, *csm4*Δ, and *csm4-3*, respectively).

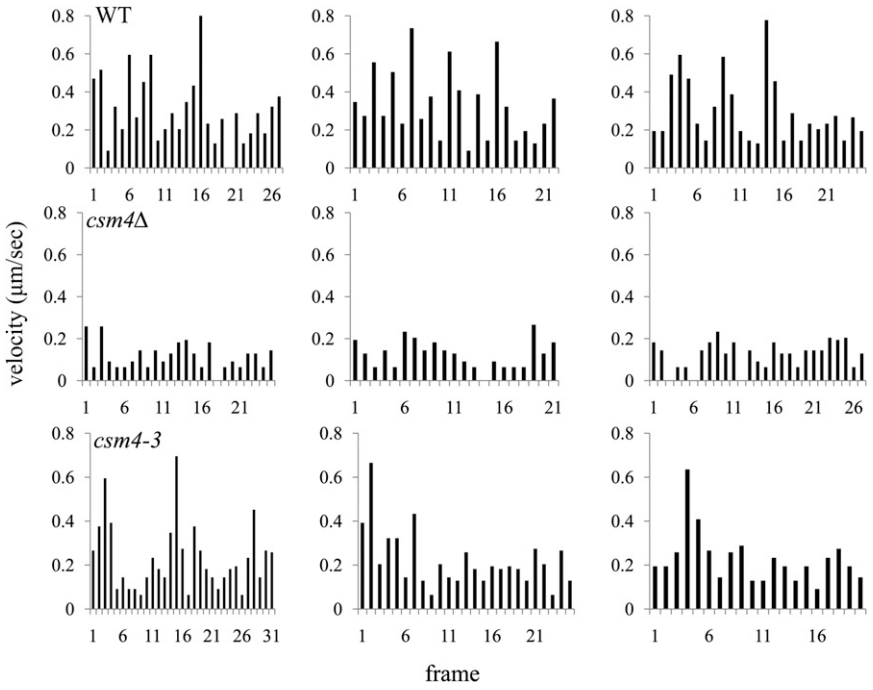

FIGURE 5.—*csm4-3* strains display occasional rapid chromosome movements. Chromosome velocity was measured in consecutive 1-sec intervals for three representative chromosomes in WT, *csm4*Δ, and *csm4-3* strains expressing Zip1-GFP.

(see below and DISCUSSION). To further understand the role of Csm4 in meiotic recombination, we tested the effect of the *pch2*Δ mutation on the spore viability of *csm4-3* and *csm4*Δ mutants. Pch2 is a meiotic protein proposed to play a role in the crossover/noncrossover decision, as well as in suppressing inappropriate repair of double strand breaks (JOSHI *et al.* 2009; ZANDERS and ALANI 2009; S. ZANDERS, M. SONNTAG BROWN, C. CHEN, and E. ALANI, unpublished observations). *pch2*Δ mutants, which maintain WT levels of spore viability, are defective in crossover interference and have very high levels of crossing over (ZANDERS and ALANI 2009). If *csm4-3* is more effective in the repair of recombination intermediates than *csm4*Δ due to higher levels of chromosome motion and pairing, one might expect *csm4-3 pch2*Δ to show higher spore viability relative to *csm4*Δ *pch2*Δ. As shown in Table 2 and Figure S4, the *pch2*Δ mutation conferred a more severe effect on spore viability in *csm4*Δ strains (31% spore viability in *csm4*Δ *pch2*Δ, a 53% decrease from *csm4*Δ) compared to *csm4-3* strains (56% spore viability in *csm4-3 pch2*Δ,

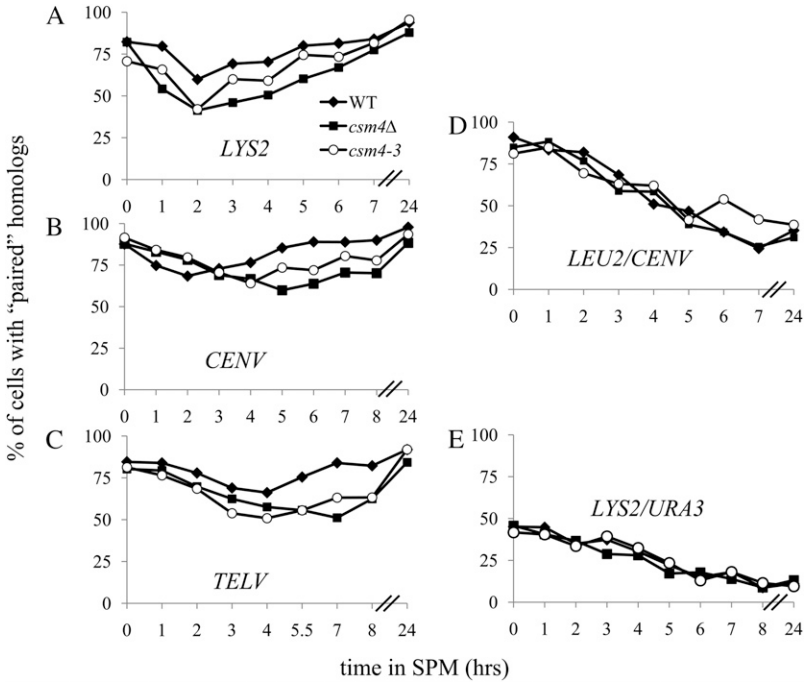

FIGURE 6.—Chromosome pairing is defective in *csm4*Δ and to a lesser extent *csm4-3*. Chromosome pairing was assayed as described in Figure 1 for *csm4-3* strains. (A, B, and C) Representative time courses with *tetO* arrays at *LYS2* (A), *CENV* (B), and *TELV* (C). Pairing was considered maximum in these *ndt80*Δ strains at $T = 24$ hr. (D and E) Representative time courses demonstrating nonhomologous pairing, with one *tetO* array at *LEU2* and another at *CENV* (D) and one at *LYS2* and another at *URA3* (E). Data from Figure 1 for WT and *csm4*Δ are shown for comparison purposes.

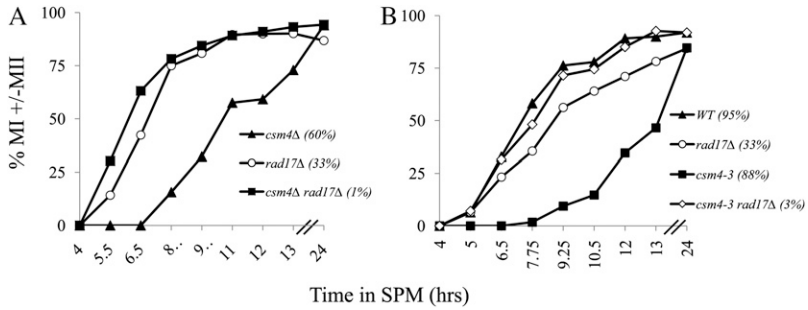

FIGURE 7.—The meiotic delays observed in *csm4*Δ and *csm4-3* are fully rescued by the *rad17*Δ mutation. Meiosis I completion (MI ± MII) time course experiments are shown for the indicated mutant strains. The spore viability of each strain is shown in parentheses following the genotype. (A and B) Representative time courses showing that a null mutation in *RAD17*, a DNA-damage checkpoint protein, rescues the meiotic delay of *csm4*Δ (A) and *csm4-3* (B). See MATERIALS AND METHODS for details.

a 36% decrease from *csm4-3*). Both double mutants showed a spore viability pattern indicative of MI nondisjunction (Figure S4). Genetic map distances, as measured on chromosome XV, were much higher than WT in tetrads of *csm4-3 pch2*Δ and single spore data of *csm4*Δ *pch2*Δ (Table 2 and data not shown). This is expected because both *csm4-3* and *pch2*Δ single mutants show increased crossing over (Table 2). These data suggest that a lack of crossing over is not likely to be the cause of low spore viability in *csm4*Δ *pch2*Δ. In the DISCUSSION we interpret the *csm4 spo11-HA/yf* and *csm4 pch2*Δ analyses to suggest that chromosome motion is important for facilitating the MI division by controlling the *placement* of crossovers between homologs.

DISCUSSION

In this study we analyzed two mutants, *csm4*Δ and *csm4-3*, that show defects in telomere-led chromosome motions during meiotic prophase in baker's yeast. Using the one-dot/two-dot tetR-GFP pairing assays, we found that both mutants showed delays in homolog pairing, with *csm4*Δ strains displaying more severe delays. Analysis of *csm4-3* mutants in chromosome motion assays suggest that fast moving chromosomes could play an important role in homolog pairing and that the timing of pairing is likely to be important for meiotic progression.

At least two hypotheses have been proposed to explain the role of chromosome motion in baker's yeast meiosis. In one model, motion is important to directly pull apart nonhomologous interactions between chromosomes, such as nonhomologous pairings or interlocks that occur during SC formation (RASMUSSEN 1986; SCHERTHAN *et al.* 1994; WANAT *et al.* 2008; STORLAZZI *et al.* 2010). Our data appear inconsistent with motion being necessary to pull apart nonhomologous pairings, since in this view we would have expected either less and/or a delay in nonhomologous "unpairings" in

TABLE 2

Spore viabilities and genetic map distances of *csm4*Δ and *csm4-3* mutants in the presence and absence of *rad17*Δ, *spo11-HA*, *spo11-HA/yf*, and *pch2*Δ mutations

Strain	% spore viability (*n*)	Cumulative distance for indicated chromosome (cM)			
		XV	III	VII	VIII
EAY1108/EAY1112 derived strains					
WT[a]	97 (1068)	101			
*csm4*Δ[a]	65 (531)	146			
csm4-3	88 (238)	126			
*rad17*Δ	33 (100)	ND			
*csm4*Δ *rad17*Δ	1 (40)	ND			
*csm4-3 rad17*Δ	3 (120)	ND			
*pch2*Δ[b]	98 (1015)	152			
*csm4*Δ *pch2*Δ	31 (200)	ND			
*csm4-3 pch2*Δ	56 (300)	167			
NH942/NH943 derived strains					
WT[a]	90 (491)		41	63	46
*csm4*Δ[a]	60 (559)		43	90	54
csm4-3	77 (180)		51	102	57
spo11-HA/yf[c]	76 (60)		29	71	49
*csm4*Δ *spo11-HA/yf*	39 (200)		ND	ND	ND
csm4-3 spo11-HA/yf	63 (300)		33	75	52

Spore viabilities and cumulative map distances were determined from tetrad data (Table S2 and Table S3). The number of tetrads dissected (*n*) to determine map distances is shown.
[a]Map distance and SV data from WANAT *et al.* (2008).
[b]Map distance and spore viability data from ZANDERS and ALANI (2009).
[c]Map distance data from MARTINI *et al.* (2006).

*csm4*Δ, which were not observed (Figure 1, D and E; Figure 6, D and E). At present, we do not have a suitable assay to monitor whether interlocks form during SC formation in baker' yeast, and if they did, whether they occur more frequently in *csm4*Δ or *csm4-3*. In a second model, fast chromosome movements contribute to pairing. Telomere-led chromosome movements could directly contribute to homolog pairing by bringing homologs together. They could also contribute indirectly by freeing chromosomes from inappropriate interactions, such as interlocks (described above). One observation that argues against the former possibility is that DSBs have been shown at one recombination hotspot, *HIS4::LEU2*, to have already engaged the homolog at the onset of zygotene, when chromosome motion initiates (Hunter and Kleckner 2001; Zickler 2006; Koszul *et al.* 2008). However, it is unclear whether this hotspot is representative of the entire genome. The back and forth motion typically seen in telomere-led chromosome motion is more consistent with the pulling apart of unwanted interactions rather than facilitating pairing (see arguments in Wanat *et al.* 2008 and as reported in Conrad *et al.* 2008; Koszul *et al.* 2008). It is important to note that some studies suggest that chromosome motion takes place prior to zygotene; for example, Parvinen and Soderstrom (1976) observed chromosome movements in rat spermatocytes in leptotene, and, in *S. cerevisiae*, movements were seen in leptotene in cells containing Rap1-GFP tagged chromosomes (Trelles-Sticken *et al.* 2005). Regardless of when motion initiates, our data show that chromosome motion is important for homolog pairing, directly and/or indirectly through removing inappropriate interactions.

Genetic analyses of *csm4* mutations analyzed in combination with mutations that affect recombination (*spo11* and *pch2*) suggest that a lack of crossovers is not the cause of the low spore viability seen in *csm4*Δ *spo11-HA/yf* and *csm4*Δ *pch2*Δ (Table 2; Figure S4). We suggest that chromosome motion regulates the placement of crossovers that facilitate MI. This idea is supported by two previous studies in baker's yeast. Rockmill *et al.* (2006) showed that defects in crossover placement in *sgs1* mutants caused a significant increase in chromosome missegregation, primarily through precocious separation of sister chromatids. Wanat *et al.* (2008) found evidence of an altered distribution of crossovers in *csm4*Δ cells that underwent chromosome III MI nondisjunction compared to those with normal disjunction. On the basis of these observations and our data, we suggest that the increased chromosome motion seen in *csm4-3* is important for crossover placements that promote an accurate MI division. Testing the crossover placement model in greater detail will require either genome-wide molecular methods (*e.g.*, Mancera *et al.* 2008) or more completely marked chromosomes.

It is important to note that the synthetic defects in spore viability observed in *csm4*Δ *spo11-HA/yf* and *csm4*Δ *pch2*Δ could also be explained by fast moving chromosomes being necessary to remove SC interlocks, as discussed above. The *pch2*Δ mutation affects the localization of the SC components Hop1 and Zip1 on meiotic chromosomes (San-Segundo and Roeder 1999; Börner *et al.* 2008), and *spo11* hypomorphs also show defects in the SC (Henderson and Keeney 2004). If residual interlocks remain in *csm4*Δ cells, challenging these cells with additional SC defects could be detrimental, leading to the decreased spore viabilities seen in *csm4*Δ *pch2*Δ and *csm4*Δ *spo11-HA/yf*.

S. pombe mutants defective in chromosome motion show a much more severe defect in meiosis than analogous mutants in budding yeast (Scherthan *et al.* 1994; Miki *et al.* 2004; Chikashige *et al.* 2006). This difference in phenotype illustrates the different requirements for chromosome motion in the two organisms. In contrast to budding yeast, fission yeast lack both synaptonemal complex (SC) and crossover interference. One possibility is that in organisms that lack SC chromosome motions play a more critical role in promoting homolog interactions. If chromosome motions are important for crossover placement, as suggested above, a more severe defect in meiosis might be expected in organisms that lack crossover interference. In budding yeast, which contains chromosomes as small as 230 kb, crossover interference plays an important role in ensuring widely spaced crossovers on all chromosomes (reviewed in Martinez-Perez and Colaiácovo 2009). Chromosome motion may be less critical in regulating crossover placement in this system, because crossover interference could presumably perform this role, though less efficiently when chromosome motion is absent. Chromosome motion in budding yeast could thus serve as a backup to crossover interference, providing another way to promote pairing and disjunction on small chromosomes. Such a model explains the more severe spore viability defect seen in *pch2*Δ *csm4*Δ mutants that are defective in both crossover interference and motion. Thus the presence of the SC could strengthen/confirm interactions between homologous chromosomes that promote crossover placement and disjunction. In other organisms, such as *pombe*, that lack SC, chromosome motion would then play a more primary role in chromosome pairing and crossover placement.

We are grateful to Angelika Amon, Nancy Kleckner, and Scott Keeney for yeast strains; Beth Weiner and Nancy Kleckner for microscopy training and providing GFP strains; Paula Cohen for the use of her Zeiss microscope for initial studies; and Damien Garbett for advice on tracking chromosome movement. We also thank Anthony Bretscher, Jen Wanat, and members of the Alani laboratory for helpful advice and comments on the manuscript. This work was supported by National Institutes of Health (NIH) grant GM53085 to E.A. supplemented with an American Recovery and Reinvestment Act of 2009 award. M.S.B. was supported by a Biochemistry, Cell, and

Molecular Biology NIH training grant and S.Z. was supported by a Cornell Presidential fellowship and a Genetics and Development NIH training grant.

LITERATURE CITED

Alexandru, G., F. Uhlmann, K. Mechtler, M. A. Poupart and K. Nasmyth, 2001 Phosphorylation of the cohesin subunit Scc1 by Polo/Cdc5 kinase regulates sister chromatid separation in yeast. Cell **105:** 459–472.

Allers, T., and M. Lichten, 2001 Intermediates of yeast meiotic recombination contain heteroduplex DNA. Mol. Cell **8:** 225–231.

Argueso, J. L., A. W. Kijas, S. Sarin, J. Heck, M. Waase *et al.*, 2003 Systematic mutagenesis of the *Saccharomyces cerevisiae* MLH1 gene reveals distinct roles for Mlh1p in meiotic crossing over and in vegetative and meiotic mismatch repair. Mol. Cell. Biol. **23:** 873–886.

Argueso, J. L., J. Wanat and Z. Gemici, 2004 Competing crossover pathways act during meiosis in *Saccharomyces cerevisiae*. Genetics **168:** 1805–1816.

Bass, W. H., 2003 Telomere dynamics unique to meiotic prophase: formation and significance of the bouquet. Cell. Mol. Life Sci. **60:** 2319–2324.

Belgareh, N., and V. Doye, 1997 Dynamics of nuclear pore distribution in nucleoporin mutant yeast cells. J. Cell Biol. **136:** 747–759.

Börner, G. V., N. Kleckner and N. Hunter, 2004 Crossover/noncrossover differentiation, synaptonemal complex formation, and regulatory surveillance at the leptotene/zygotene transition of meiosis. Cell **117:** 29–45.

Börner, G. V., A. Barot and N. Kleckner, 2008 Yeast Pch2 promotes domainal axis organization, timely recombination progression, and arrest of defective recombinosomes during meiosis. Proc. Natl. Acad. Sci. USA **105:** 3327–3332.

Brar, G. A., A. Hochwagen, L. S. Ee and A. Amon, 2009 The multiple roles of cohesin in meiotic chromosome morphogenesis and pairing. Mol. Biol. Cell **20:** 1030–1047.

Buhler, C., V. Borde and M. Lichten, 2007 Mapping meiotic single-strand DNA reveals a new landscape of DNA double-strand breaks in *Saccharomyces cerevisiae*. PLoS Biol **5:** e324.

Burgess, S. M., N. Kleckner and B. M. Weiner, 1999 Somatic pairing of homologs in budding yeast: existence and modulation. Genes Dev **13:** 1627–1641.

Chikashige, Y., C. Tsutsumi, M. Yamane, K. Okamasa, T. Haraguchi *et al.*, 2006 Meiotic proteins Bqt1 and Bqt2 tether telomeres to form the bouquet arrangement of chromosomes. Cell **125:** 59–69.

Chikashige, Y., T. Haraguchi and Y. Hiraoka, 2007 Another way to move chromosomes. Chromosoma **116:** 497–505.

Chua, P. R., and G. S. Roeder, 1997 Tam1, a telomere-associated meiotic protein, functions in chromosome synapsis and crossover interference. Genes Dev **11:** 1786–1800.

Chua, P. R., and G. S. Roeder, 1998 Zip2, a meiosis-specific protein required for the initiation of chromosome synapsis. Cell **93:** 349–359.

Conrad, M. N., A. M. Dominguez and M. E. Dresser, 1997 Ndj1p, a meiotic telomere protein required for normal chromosome synapsis and segregation in yeast. Science **276:** 1252–1255.

Conrad, M. N., C. Y. Lee, J. L. Wilkerson and M. E. Dresser, 2007 MPS3 mediates meiotic bouquet formation in *Saccharomyces cerevisiae*. Proc. Natl. Acad. Sci. USA **104:** 8863–8868.

Conrad, M. N., C. Y. Lee, G. Chao, M. Shinohara, H. Kosaka *et al.*, 2008 Rapid telomere movement in meiotic prophase is promoted by NDJ1, MPS3, and CSM4 and is modulated by recombination. Cell **133:** 1175–1187.

Davis, L., and G. R. Smith, 2006 The meiotic bouquet promotes homolog interactions and restricts ectopic recombination in *Schizosaccharomyces pombe*. Genetics **174:** 167–177.

de los Santos, T., N. Hunter, C. Lee, B. Larkin, J. Loidl *et al.*, 2003 The Mus81/Mms4 endonuclease acts independently of double-Holliday junction resolution to promote distinct subset of crossovers during meiosis in budding yeast. Genetics **164:** 81–94.

Diaz, R. L., A. D. Alcid, J. M. Berger and S. Keeney, 2002 Identification of residues in yeast Spo11p critical for meiotic DNA double-strand break formation. Mol. Cell. Biol. **22:** 1106–1115.

Galbraith, A. M., S. A. Bullard, K. Jiao, J. J. Nau and R. E. Malone, 1997 Recombination and the progression of meiosis in *Saccharomyces cerevisiae*. Genetics **146:** 481–489.

Gietz, R. D., R. H. Schiestl, A. R. Willems and R. A. Woods, 1995 Studies on the transformation of intact yeast cells by the LiAc/SS-DNA/PEG procedure. Yeast **11:** 355–360.

Goldman, A. S., and M. Lichten, 2000 Restriction of ectopic recombination by interhomolog interactions during *Saccharomyces cerevisiae* meiosis. Proc. Natl. Acad. Sci. USA **97:** 9537–9542.

Goldstein, A. L., and J. H. Mccusker, 1999 Three new dominant drug resistance cassettes for gene disruption in *Saccharomyces cerevisiae*. Yeast **15:** 1541–1553.

Golubovskaya, I. N., L. C. Harper, W. P. Pawlowski, D. Schichnes and W. Z. Cande, 2002 The *pam1* gene is required for meiotic bouquet formation and efficient homologous synapsis in maize (*Zea mays L.*). Genetics **162:** 1979–1993.

Grushcow, J. M., T. M. Holzen, K. J. Park, T. T. Weinert, M. Lichten *et al.*, 1999 *Saccharomyces cerevisiae* checkpoint genes *MEC1, RAD17*, and *RAD24* are required for normal meiotic recombination partner choice. Genetics **153:** 607–620.

Harper, L., I. Golubovskaya and W. Z. Cande, 2004 A bouquet of chromosomes. J. Cell Sci **117:** 4025–4032.

Hassold, T., and P. Hunt, 2001 To err (meiotically) is human: the genesis of human aneuploidy. Nat. Rev. Genet. **2:** 280–291.

Henderson, K. A., and S. Keeney, 2004 Tying synaptonemal complex initiation to the formation and programmed repair of DNA double-strand breaks. Proc. Natl. Acad. Sci. USA **101:** 4519–4524.

Hunter, N., and N. Kleckner, 2001 The single-end invasion: an asymmetric intermediate at the double-strand break to double-holliday junction transition of meiotic recombination. Cell **106:** 59–70.

Joseph, I., and A. J. Lustig, 2007 Telomeres in meiotic recombination: the yeast side story. Cell. Mol. Life Sci. **64:** 125–130.

Joshi, N., A. Barot, C. Jamison and G. V. Börner, 2009 Pch2 links chromosome axis remodeling at future crossover sites and crossover distribution during yeast meiosis. PLoS Genet **5:** e1000557.

Keeney, S., 2001 Mechanism and control of meiotic recombination initiation Curr. Top. Dev. Biol. **52:** 1–53.

Kosaka, H., M. Shinohara and A. Shinohara, 2008 Csm4-dependent telomere movement on nuclear envelope promotes meiotic recombination. PLoS Genet **4:** e1000196.

Koszul, R., K. Kim, M. Prentiss, N. Kleckner and S. Kameoka, 2008 Meiotic chromosomes move by linkage to dynamic actin cables with transduction of force through the nuclear envelope. Cell **133:** 1188–1201.

Koszul, R., S. Kameoka and B. M. Weiner, 2009 Real-time imaging of meiotic chromosomes in *Saccharomyces cerevisiae*. Methods Mol. Biol. **558:** 81–89.

Lacefield, S., and A. W. Murray, 2007 The spindle checkpoint rescues the meiotic segregation of chromosomes whose crossovers are far from the centromere. Nat. Genet. **39:** 1273–1277.

Lao, J. P., S. D. Oh, M. Shinohara, A. Shinohara and N. Hunter, 2008 Rad52 promotes postinvasion steps of meiotic double-strand-break repair. Mol. Cell **9:** 517–524.

Loidl, J., F. Klein and H. Scherthan, 1994 Homologous pairing is reduced but not abolished in asynaptic mutants of yeast. J. Cell Biol. **125:** 1191–1200.

Lydall, D., Y. Nikolsky, D. K. Bishop and T. A. Weinert, 1996 A meiotic recombination checkpoint controlled by mitotic checkpoint genes. Nature **383:** 840–843.

Mancera, E., R. Bourgon, A. Brozzi, W. Huber and L. M. Steinmetz, 2008 High-resolution mapping of meiotic crossovers and non-crossovers in yeast. Nature **454:** 479–485.

Marston, A. L., W. H. Tham, H. Shah and A. Amon, 2004 A genome-wide screen identifies genes required for centromeric cohesion. Science **303:** 367–370.

Martinez-Perez, E., and M. P. Colaiácovo, 2009 Distribution of meiotic recombination events: talking to your neighbors. Curr. Opin. Genet. Dev. **19:** 105–112.

Martini, E., R. L. Diaz, N. Hunter and S. Keeney, 2006 Crossover homeostasis in yeast meiosis. Cell **126:** 285–295.

Miki, F., A. Kurabayashi, Y. Tange, K. Okazaki, M. Shimanuki *et al.*, 2004 Two- hybrid search for proteins that interact with Sad1 and Kms1, two membrane-bound components of the spindle pole body in fission yeast. Mol. Genet. Genomics **270:** 449–461.

Niwa, O., M. Shimanuki and F. Miki, 2000 Telomere-led bouquet formation facilitates homologous chromosome pairing and restricts ectopic interaction in fission yeast meiosis. EMBO J. **19:** 3831–3840.

Page, S. L., and R. S. Hawley, 2004 The genetics and molecular biology of the synaptonemal complex. Annu. Rev. Cell Dev. Biol. **20:** 525–558.

Parvinen, M., and K. O. Soderstrom, 1976 Chromosome rotation and formation of synapsis. Nature **260:** 534–535.

Peoples, T. L., E. Dean, O. Gonzalez, L. Lambourne and S. M. Burgess, 2002 Close, stable homolog juxtaposition during meiosis in budding yeast is dependent on meiotic recombination, occurs independently of synapsis, and is distinct from DSB- independent pairing contacts. Genes Dev. **16:** 1682–1695.

Rabitsch, K. P., A. Tóth, M. Gálová, A. Schleiffer, G. Schaffner *et al.*, 2001 A screen for genes required for meiosis and spore formation based on whole-genome expression. Curr. Biol. **11:** 1001–1009.

Rasmussen, S. W., 1986 Chromosome interlocking during synapsis-a transient disorder. Tokai J. Exp. Clin. Med. **11:** 437–451.

Rockmill, B., and G. S. Roeder, 1998 Telomere-mediated chromosome pairing during meiosis in budding yeast. Genes Dev. **12:** 2574–2586.

Rockmill, B., K. Voelkel-Meiman and G. S. Roeder, 2006 Centromere-proximal crossovers are associated with precocious separation of sister chromatids during meiosis in *Saccharomyces cerevisiae*. Genetics **174:** 1745–1754.

Roeder, G. S., 1997 Meiotic chromosomes: it takes two to tango. Genes Dev. **11:** 2600–2621.

Rose, M. D., F. Winston and P. Hieter, 1990 *Methods in Yeast Genetics: A Laboratory Course Manual*, Cold Spring Harbor Laboratory Press, Cold Spring Harbor, NY.

San-Segundo, P. A., and G. S. Roeder, 1999 Pch2 links chromatin silencing to meiotic checkpoint control. Cell **97:** 313–324.

Sato, A., B. Isaac, C. M. Phillips, R. Rillo, P. M. Carlton *et al.*, 2009 Cytoskeletal forces span the nuclear envelope to coordinate meiotic chromosome pairing and synapsis. Cell **139:** 907–919.

Scherthan, H., J. Bahler and J. Kohli, 1994 Dynamics of chromosome organization and pairing during meiotic prophase in fission yeast. J. Cell Biol. **127:** 273–285.

Scherthan, H., S. Weich, H. Schwegler, C. Heyting, M. Härle *et al.*, 1996 Centromere and telomere movements during early meiotic prophase of mouse and man are associated with the onset of chromosome pairing. J. Cell Biol. **134:** 1109–1125.

Scherthan, H., H. Wang, C. Adelfalk, E. J. White, C. Cowan *et al.*, 2007 Chromosome mobility during meiotic prophase in *Saccharomyces cerevisiae*. Proc. Natl. Acad. Sci. USA **104:** 16934–16939.

Schwacha, A., and N. Kleckner, 1995 Identification of double Holliday junctions as intermediates in meiotic recombination. Cell **83:** 783–791.

Storlazzi, A., S. Gargano, G. Ruprich-Robert, M. Falque, M. David *et al.*, 2010 Recombination proteins mediate meiotic spatial organization and pairing. Cell **141:** 94–106.

Tóth, A., K. P. Rabitsch, M. Gálová, A. Schleiffer, S. B. Buonomo *et al.*, 2000 Functional genomics identifies monopolin: a kinetochore protein required for segregation of homologs during meiosis I. Cell **103:** 1155–1168.

Trelles-Sticken, E., J. Loidl and H. Scherthan, 1999 Bouquet formation in budding yeast: initiation of recombination is not required for meiotic telomere clustering. J. Cell Sci. **112:** 651–658.

Trelles-Sticken, E., M. E. Dresser and H. Scherthan, 2000 Meiotic telomere protein Ndj1p is required for meiosis-specific telomere distribution, bouquet formation and efficient homologue pairing. J. Cell Biol. **151:** 95–106.

Trelles-Sticken, E., C. Adelfalk, J. Loidl and H. Scherthan, 2005 Meiotic telomere clustering requires actin for its formation and cohesin for its resolution. J. Cell Biol. **170:** 213–223.

Tsubouchi, H., and G. S. Roeder, 2003 The importance of genetic recombination for fidelity of chromosome pairing in meiosis. Dev. Cell **5:** 915–925.

Wach, A., A. Brachat, R. Pohlmann and P. Philippsen, 1994 New heterologous modules for classical or PCR-based gene disruptions in *Saccharomyces cerevisiae*. Yeast **10:** 1793–1808.

Wanat, J. J., K. P. Kim, R. Koszul, S. Zanders, B. Weiner *et al.*, 2008 Csm4, in collaboration with Ndj1, mediates telomere-led chromosome dynamics and recombination during yeast meiosis. PLoS Genet. **4:** e1000188.

Weiner, B. M., and N. Kleckner, 1994 Chromosome pairing via multiple interstitial interactions before and during meiosis in yeast. Cell **77:** 977–991.

Wu, H. Y., and S. M. Burgess, 2006 Ndj1, a telomere-associated protein, promotes meiotic recombination in budding yeast. Mol. Cell. Biol. **26:** 3683–3694.

Wu, H. Y., H. C. Ho and S. M. Burgess, 2010 Mek1 kinase governs outcomes of meiotic recombination and the checkpoint response. Curr. Biol. **20:** 1707–1716.

Yamamoto, A., R. R. West, J. R. McIntosh and Y. Hiraoka, 1999 A cytoplasmic dynein heavy chain is required for oscillatory nuclear movement of meiotic prophase and efficient meiotic recombination in fission yeast. J. Cell Biol. **145:** 1233–1249.

Yang, H. D., and L. A. Pon, 2002 Actin cable dynamics in budding yeast. Proc. Natl. Acad. Sci. USA **99:** 751–756.

Zanders, S., and E. Alani, 2009 The *pch2Delta* mutation in baker's yeast alters meiotic crossover levels and confers a defect in crossover interference. PLoS Genet **5:** e1000571.

Zickler, D., 2006 From early homologue recognition to synaptonemal complex formation. Chromosoma **115:** 158–174.

Zickler, D., and N. Kleckner, 1999 Meiotic chromosomes: integrating structure and function. Annu. Rev. Genet. **33:** 603–754.

Communicating editor: N. M. Hollingsworth

GENETICS

Supporting Information
http://www.genetics.org/cgi/content/full/genetics.110.125575/DC1

Sustained and Rapid Chromosome Movements Are Critical for Chromosome Pairing and Meiotic Progression in Budding Yeast

Megan Sonntag Brown, Sarah Zanders and Eric Alani

Copyright © 2011 by the Genetics Society of America
DOI: 10.1534/genetics.110.125575

FIGURE S1.—Representative images for one-dot/two-dot cells. Cells with one (paired, top) and two (unpaired, bottom) *tetO/tetR-GFP* dots are shown.

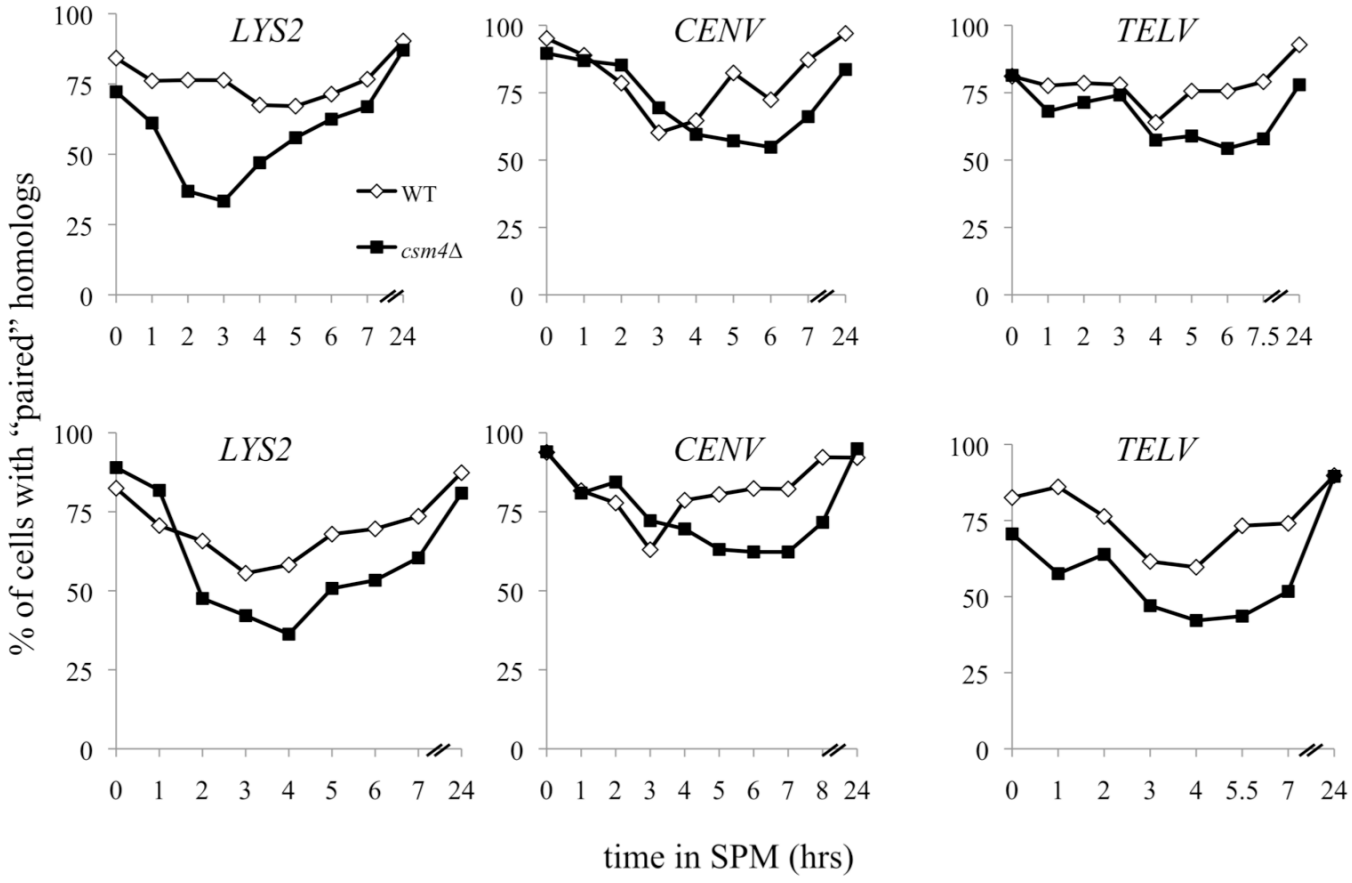

FIGURE S2.—Additional time courses for WT and *csm4Δ* with *tetO* arrays at *LYS2, CENV,* and *TELV*. See Figure 1 for details.

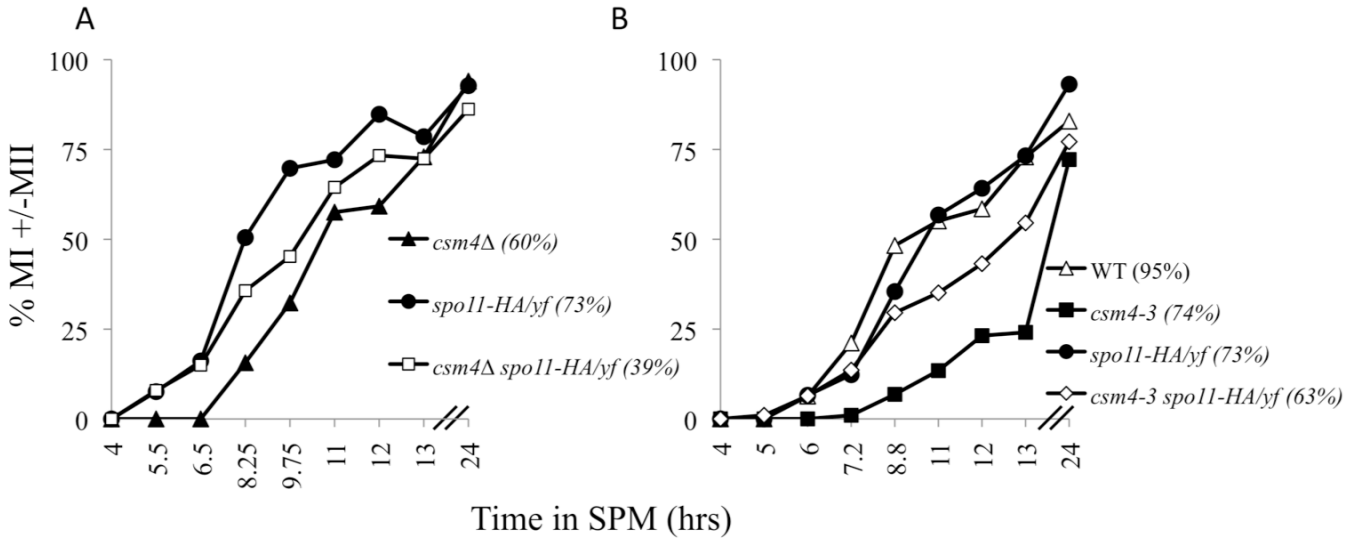

FIGURE S3.—The meiotic delays observed in *csm4Δ* and *csm4-3* are partially rescued by a *spo11* hypomorph mutation. (A, B) Representative time courses showing that a *spo11* hypomorph, *spo11-HA/yf,* can partially rescue the meiotic delay, as measured by completion of MI (MI +/- MII) of *csm4Δ* (panel A) and *csm4–3* (panel B).

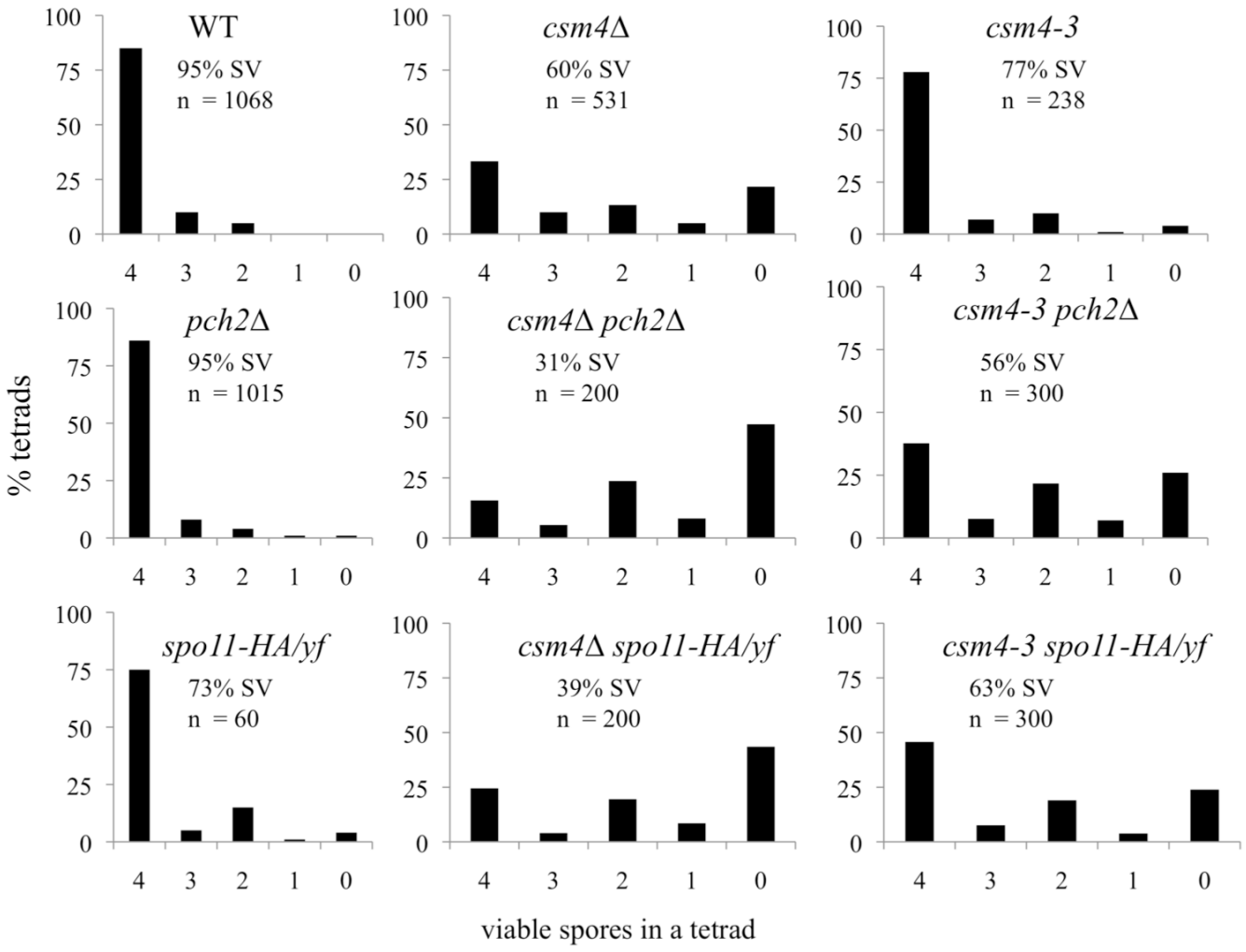

FIGURE S4.—Spore viability profile of wild-type and mutant strains. The vertical axis shows the percentage of each tetrad class and the horizontal axis represents the number of viable spores in a tetrad. SV: percentage spore viability; n: total number of tetrad dissected. Data are a graphical representation of Table 2.

TABLE S1

Yeast strains used in this study

Strain Names	Genotype
NH943	*MATa, ho::hisG, ade2Δ, ura3(ΔSma-Pst), leu2::hisG, CEN3::ADE2, lys5-P, cyh2^r, his4-B*
SKY665	as NH943 except *MATα, spo11(Y135F)-HA3His6::KANMX4*
EAY3036	as NH943 except *MATα, spo11(Y135F)-HA3His6::KANMX4, csm4Δ::HPHMX4*
EAY1483	as NH943 except *csm4Δ::KANMX4*
NH942	*MATα, ho::hisG, ade2Δ, can1, ura3(ΔSma-Pst), met13-B, trp5-S, CEN8::URA3, thr1-A, cup1^s*
SKY633	as NH942 except *MATa, spo11-HA3His6::KANMX4*
EAY3037	as NH942 except *MATa, spo11-HA3His6::KANMX4, csm4Δ::HPHMX4*
EAY3038	as NH942 except *MATa, spo11-HA3His6::KANMX4, csm4(K22A;K24A)::KANMX4*
EAY1484	as NH942 except *csm4Δ::KANMX4*
EAY3039	as NH942 except *csm4(K22A;K24A)::KANMX4*
EAY1108	*MATa, ho::hisG, lys2, ura3, leu2::hisG, trp1::hisG, URA3-CEN15, iLEU2-chXV, iLYS2-chXV*
EAY1480	as EAY1108, but *csm4Δ::HPHMX4*
EAY1977	as EAY1108 but *csm4Δ::KANMX4*, *pch2Δ::NATMX4*
EAY3041	as EAY1108 but *csm4(K22A;K24A)::KANMX4, pch2Δ::NATMX4*
EAY1981	as EAY1108, but *csm4Δ::KANMX4, rad17Δ::HPHMX4*
EAY3040	as EAY1108 but *csm4(K22A;K24A)::KANMX4, rad17Δ::HPHMX4*
EAY2885	as EAY1108, but *csm4(K22A;K24A)::KANMX4*
EAY2887	as EAY1108, but *csm4(D40A)::KANMX4*
EAY2888	as EAY1108, but *csm4(E80A)::KANMX4*
EAY2890	as EAY1108, but *csm4(K96A)::KANMX4*
EAY2891	as EAY1108, but *csm4(E100A)::KANMX4*
EAY2889	as EAY1108, but *csm4(D123A;E124A)::KANMX4*
EAY2886	as EAY1108, but *csm4(E155A)::KANMX4*

EAY1112	*MATα, ho::hisG, lys2, ura3, leu2::hisG, trp1::hisG, ade2::hisG, his3::hisG, TRP1-CEN15*
EAY1481	as EAY1112, but *csm4*Δ::*HPHMX4*
EAY1978	as EAY1112, but *csm4*Δ::*KANMX4*, *pch2*Δ::*NATMX4*
EAY1982	as EAY1112, but *csm4*Δ::*KANMX4, rad17*Δ.::*HPHMX4*
EAY3042	*MATa, ho::hisG, leu2::hisG, URA3::NUP49-GFP-URA3*
YKK254/EAY2151	*MATa, ho::hisG, leu2::hisG, URA3::NUP49-GFP-URA3 , csm4*Δ*::HPHMX4*
EAY2225	as EAY3042 except *csm4(D3A)::KANMX4*
EAY3044	as EAY3042 except *csm4(R8A;K9A)::KANMX4*
EAY2223	as EAY3042 except *csm4(K22A;K24A)::KANMX4*
EAY2235	as EAY3042 except *csm4(E31A;R32A;K33A)::KANMX4*
EAY2233	as EAY3042 except *csm4(D40A)::KANMX4*
EAY3045	as EAY3042 except *csm4(D47A)::KANMX4*
EAY2227	as EAY3042 except *csm4(E54A)::KANMX4*
EAY2220	as EAY3042 except *csm4(K57A;K59A;E60A)::KANMX4*
EAY2241	as EAY3042 except *csm4(E66A)::KANMX4*
EAY3046	as EAY3042 except *csm4(E80A)::KANMX4*
EAY2229	as EAY3042 except *csm4(D83A;R84A;E85A)::KANMX4*
EAY2237	as EAY3042 except *csm4(D92A;D93A)::KANMX4*
EAY2239	as EAY3042 except *csm4(K96A)::KANMX4*
EAY2249	as EAY3042 except *csm4(E100A)::KANMX4*
EAY2221	as EAY3042 except *csm4(K109A;R111A)::KANMX4*
EAY2245	as EAY3042 except *csm4(D123A;E124A)::KANMX4*
EAY2217	as EAY3042 except *csm4(H128A;K130A)::KANMX4*
EAY2243	as EAY3042 except *csm4(E135A)::KANMX4*
EAY2231	as EAY3042 except *csm4(E155A)::KANMX4*
EAY3043	*MATα, ho::hisG, leu2::hisG, URA3::NUP49-GFP-URA3*
YKK255	*MATα, ho::hisG, leu2::hisG, URA3::NUP49-GFP-URA3 , csm4*Δ*::HPHMX4*
YKK713	*MATa, ho::hisG, leu2::hisG, ZIP1::ZIP1-GFP(700), ura3, csm4*Δ*::HPHMX4*
EAY3047	*MATa, ho::hisG, leu2::hisG, ZIP1::ZIP1-GFP(700), ura3*

EAY3049	*MATa, ho::hisG, leu2::hisG, ZIP1::ZIP1-GFP(700), ura3, csm4(K22A;K24A)::KANMX4*
YKK720	*MATα, ho::hisG, leu2::hisG, ZIP1::ZIP1-GFP(700), ura3, csm4Δ::HPHMX4*
EAY3048	*MATα, ho::hisG, leu2::hisG, ZIP1::ZIP1-GFP(700), ura3*
A9785	*MATa ho::LYS2, ura3, his3::hisG, trp1::hisG, lys2::TetOx240:URA3, leu2::LEU2-tetR-GFP, ndt80Δ::PSTE5:URA3*
EAY2995	as EAY2985 except *csm4Δ::HPHMX4*
A9786/EAY2984	*MATα ho::LYS2, ura3, his3::hisG, trp1::hisG, lys2::TetOx240:URA3, leu2::LEU2-tetR-GFP, ndt80Δ::PSTE5:URA3*
EAY2994	as EAY2984 except *csm4Δ::HPHMX4*
EAY3050	as EAY2984 except *csm4(K22A;K24A)::KANMX4*
A16204/EAY2987	*MATa ho::LYS2, lys2, ura3, leu2::hisG, trp1::hisG, promURA3::tetR:: GFP-LEU2, TelV::tetOx224::URA3, ndt80Δ::PSTE5:URA3*
EAY2997	as EAY2987 except *csm4Δ::HPHMX4*
A16203/EAY2988	*MATα ho::LYS2, lys2, ura3, leu2::hisG, trp1::hisG, promURA3::tetR:: GFP-LEU2, TelV::tetOx224::URA3, ndt80Δ::PSTE5:URA3*
EAY2998	as EAY2988 except *csm4Δ::HPHMX4*
EAY3051	as EAY2988 except *csm4(K22A;K24A)::KANMX4*
A16199/EAY2981	*MATa, ho::LYS2, lys2, leu2::hisG, ura3, trp1::hisG, his3::hisG, leu2::pURA3-TetR-GFP::LEU2, CENV::TetOx224::HIS3, ndt80Δ::PSTE5:URA3*
EAY2991	as EAY2981 except *csm4Δ::HPHMX4*
A16201/EAY2986	*MATα, ho::LYS2, lys2, leu2::hisG, ura3, trp1::hisG, his3::hisG, leu2::pURA3-TetR-GFP::LEU2, CENV::TetOx224::HIS3, ndt80Δ::PSTE5:URA3*
EAY2996	as EAY2986 except *csm4Δ::HPHMX4*
EAY3052	as EAY2986 except *csm4(K22A;K24A)::KANMX4*
A5047/EAY2982	*MATa, ho::LYS2, ura3, leu2::hisG, his3::hisG, trp1::hisG, leu2::LEU2::tetR-GFP::TetO-HIS3, ndt80Δ::PSTE5:URA3*
EAY2992	as EAY2982 except *csm4Δ::HPHMX4*
A5049/EAY2983	*MATα, ho::LYS2, ura3, leu2::hisG, his3::hisG, trp1::hisG, leu2::LEU2::tetR-GFP::TetO-HIS3, ndt80Δ::PSTE5:URA3*
EAY2993	as EAY2983 except *csm4Δ::HPHMX4*
EAY3053	as EAY2983 except *csm4(K22A;K24A)::KANMX4*
A6644/EAY2979	*MATa, ho::LYS2, ura3, leu2::hisG, his3::hisG, trp1::hisG, pURA3::tetR::GFP::LEU2, tetOx224::URA3, ndt80Δ::PSTE5:URA3*
EAY2989	as EAY2979 except *csm4Δ::HPHMX4*

TABLE S2

Map distances and distributions of parental and recombinant progeny for the EAY1108/1112 background

Strain	PD	TT	NPD	Map distance (cM)
URA3- LEU2:				
WT	607	456	5	21.9-23.8
*csm4*Δ	203	319	9	33.3-36.9
*CSM4/csm4*Δ	46	40	2	24.4-34.6
csm4-3	117	107	1	23.1-27.1
csm4-5	30	31	1	24.4-35.2
csm4-10	73	59	1	21.4-27.4
csm4-13	85	72	2	23.3-29.5
csm4-14	26	35	3	33.6-49.2
csm4-16	59	69	3	29.0-37.4
csm4-19	49	72	0	27.6-32.0
*pch2*Δ	563	423	18	25,0-27.8
*csm4-3 pch2*Δ	31	30	1	23.6-34.4
LEU2-LYS2:				
WT	496	569	5	26.6-28.5
*csm4*Δ	216	312	3	29.9-32.7
*CSM4/csm4*Δ	44	44	0	22.3-27.7
csm4-3	84	138	3	32.1-37.3
csm4-5	21	38	3	37.3-53.1
csm4-10	52	81	0	28.4-32.6
csm4-13	59	96	4	33.9-41.5
csm4-14	29	34	1	26.1-36.5
csm4-16	50	80	1	29.9-35.8
csm4-19	54	65	2	27.9-35.7
*pch2*Δ	395	561	39	38.2-41.8
*csm4-3 pch2*Δ	26	33	3	33.0-49.0
LYS2-ADE2:				
WT	803	263	2	12.1-13.7
*csm4*Δ	362	128	1	12.6-14.9
*CSM4/csm4*Δ	29	19	0	7.5-13.3
csm4-3	158	66	1	14.0-18.0
csm4-5	48	14	0	8.6-14.0
csm4-10	88	45	0	14.9-19.0

csm4-13	105	53	1	16.0-21.2
csm4-14	41	23	0	15.0-21.0
csm4-16	91	40	0	13.3-17.3
csm4-19	79	42	0	15.2-19.6
*pch2*Δ	649	344	7	18.2-20.4
*csm4-3 pch2*Δ	34	25	3	26.5-42.9
ADE2-HIS3:				
WT	343	709	16	36.5-38.9
*csm4*Δ	120	378	33	51.3-57.1
*CSM4/csm4*Δ	22	64	2	38.4-48.0
csm4-3	60	153	12	45.8-54.2
csm4-5	14	44	4	46.2-63.4
csm4-10	33	92	8	46.9-58.3
csm4-13	38	109	12	51.1-62.7
csm4-14	18	41	5	46.2-64.8
csm4-16	30	87	14	58.0-72.6
csm4-19	26	84	11	55.0-69.0
*pch2*Δ	243	638	115	63.9-69.5
*csm4-3 pch2*Δ	19	36	7	51.8-74.0

*pch2*Δ data are from ZANDERS and ALANI (2009). WT and *csm4*Δ tetrad data are from WANAT *et al.* (2008). All mutants are isogenic derivatives of EAY1108/EAY1112. Intervals on chromosome XV correspond to the genetic distance calculated from tetrad distribution data +/- one standard error, calculated using the Stahl Laboratory Online Tools website (http://www.molbio.uoregon.edu/~fstahl/).

TABLE S3

Map distances and distributions of parental and recombinant progeny for the NH942/943 background

Strain	PD	TT	NPD	cM
Chromosome III				
HIS4-LEU2:				
WT	669	213	3	12.2-14.0
*csm4*Δ	413	114	3	11.2-13.8
csm4-3	77	30	0	11.8-16.2
spo11yf	719	197	2	10.6-12.2
csm4-3 spo11yf	42	4	0	2.2-6.4
LEU2-CEN3:				
WT	774	128	1	6.7-8.1
*csm4*Δ	426	99	5	10.7-13.7
csm4-3	82	23	2	12.1-20.7
spo11yf	828	94	0	4.6-5.6
csm4-3 spo11yf	39	6	1	6.2-19.8
CEN3-MATa:				
WT	590	300	10	18.7-21.3
*csm4*Δ	353	173	4	17.1-20.1
csm4-3	68	38	1	17.1-24.1
spo11yf	696	221	2	11.9-13.5
csm4-3 spo11yf	32	14	0	11.8-18.6
Chromosome VII				
LYS2-MET13:				
WT	569	311	1	17.1-18.9
*csm4*Δ	288	229	6	23.6-27.0
csm4-3	54	55	3	27.8-37.4
spo11yf	603	282	3	15.9-17.9
csm4-3 spo11yf	28	18	0	16.0-23.2
MET13-CYH2:				
WT	706	182	0	9.5-10.9
*csm4*Δ	370	152	1	14.0-16.2
csm4-3	70	42	0	16.5-21.1
spo11yf	707	154	2	8.8-10.4
csm4-3 spo11yf	40	6	0	4.0-9.0
CYH2-TRP5:				
WT	364	524	18	33.5-36.5
*csm4*Δ	150	344	29	46.7-52.3

csm4-3	33	72	7	44.5-57.3
spo11yf	271	591	36	43.0-46.8
csm4-3 spo11yf	11	33	2	40.4-57.4
Chromosome VIII				
URA3-THR1:				
WT	532	330	3	19.1-21.1
*csm4*Δ	291	231	5	23.2-26.4
csm4-3	56	50	1	22.7-29.7
spo11yf	569	266	4	16.2-18.4
csm4-3 spo11yf	29	16	1	16.9-30.9
THR1-CUP1:				
WT	439	416	6	25.0-27.4
*csm4*Δ	256	263	8	27.7-31.3
csm4-3	51	54	2	26.5-35.1
spo11yf	373	453	14	30.5-33.5
csm4-3 spo11yf	28	17	1	18.0-32.0

All mutants are derivatives of NH942/NH943. WT and *spoll-HA/yf* data are from MARTINI *et al.* (2006), and *csm4*Δ data are from WANAT *et al.* (2008). Intervals were calculated as in Table S2.